

Stability, chemical bonding, and vibrational properties of amorphous carbon at different mass densities

Th. Köhler, Th. Frauenheim, and G. Jungnickel

Theoretische Physik III, Institut für Physik, Technische Universität, D-09107 Chemnitz, Germany

(Received 5 May 1995; revised manuscript received 20 June 1995)

We investigate correlations between the atomic-scale structure and the global electronic and vibrational properties in amorphous carbon versus mass density. The model structures have been generated by applying different annealing regimes using a density-functional-based nonorthogonal tight-binding molecular dynamics. The stability of the amorphous modifications and the calculated vibrational density of states (VDOS) are strongly affected by the density and the annealing sequences, altering the chemical composition, the $sp/sp^2/sp^3$ clustering, the structure, and related physical properties. A mass density of 3.0 g/cm^3 is confirmed as a magic density favoring the formation of most stable α -C modifications having lowest defect densities and maximum band gap. By projecting out different hybrid-fractional VDOS and analyzing the localization behavior we identify the spectral signatures for chemically different bonded species that may be used for comparison with related experimental work. At low density the vibrational spectra are reminiscent of graphite and clearly indicate a softening of modes due to chainlike segments and rings within a low-connectivity network. Opposite, the spectra at high density become more compact in range and rigid shifting the low-frequency bound to higher values developing a characteristic half-sphere shape. At all densities a set of localized modes at high frequency represents signs of the embedding of undercoordinated atoms in a rigid higher coordinated environment.

I. INTRODUCTION

By the successful handling of different deposition techniques, many different metastable amorphous carbon modifications have been prepared during the last two decades.¹ The thin film material spans the whole spectra of physical properties between graphite and diamond. However, there is still a large gap in the understanding of experimentally found features on the basis of atomic scale models. Whereas experimental analysis only provides a limited structural averaged insight into these problems, molecular-dynamics (MD) modeling of atomic-scale structures in comparison with related experimental (structural, diffraction, vibrational, electronic, and spectroscopic) data on the basis of a coupling between atomic and electronic degrees of freedom has become a powerful tool in elucidating structure property relations and mechanisms for structure formation.²⁻⁵

The described theoretical data that has been compared with experiments (electron and neutron diffraction, optical gap, valence band photoelectron spectra), however, in most cases represent structural averaged data of the related material properties. On their basis, the broad variation of the local chemical bonding and defect distribution is only hardly to discriminate. For practical purposes in thin film characterization, a single more local probe, which unequivocally may be related to corresponding data of atomic-scale models and simultaneously is predictive of other film properties, would be highly desirable.

Vibrational spectroscopy such as Raman and IR are well-developed room ambient tools available in many lab-

oratories, which places no constraints on substrate size and shape. Consequently, these techniques have been widely used to characterize a broad variety of amorphous, mostly hydrogenated, carbon films, deposited by various methods. For a review we refer the reader to Tamor and Vassell⁶ and to Silva, Amaratunga, and Constantinou.⁷ Due to the complete lack of systematical theoretical work in this field, the obtained experimental features are analyzed in terms of the effective medium theory comparing with the well-defined features in graphite and diamond.

To put the interpretation of the experimental data on a more profound theoretical basis, we present in this paper the calculated vibrational spectra of amorphous models generated at densities between 2.0 g/cm^3 and 3.52 g/cm^3 by two different annealing regimes using a density-functional-based tight-binding MD (TB-MD). The method for the calculation of interatomic forces and the simulation regimes used for generating the structures are briefly outlined in Sec. II. In Sec. III, we review the structural and physical properties of representative amorphous modifications and characterize their energetic stability. The global band gap properties that are determined by the detailed clustering of chemically different bonded carbon atoms^{8,9} only will be touched on in completing the discussion of the model properties. In Sec. IV, we describe the basic ideas for determining the vibrational properties, including total, partial, and local vibrational density of states (VDOS), completed by a quantitative measure in describing the localization of vibrational modes. The results obtained for all amorphous models are presented in Sec. V. We discuss the detailed changes in the vibrational spectra versus mass density that are clearly affected by the changing $sp/sp^2/sp^3$ ra-

tio and the changing cluster distribution. Concluding in Sec. VI, we compare the theoretically obtained spectral features with related Raman and IR work and give examples for soft and localized modes in amorphous carbon.

II. DENSITY-FUNCTIONAL-BASED MD

To model the structure formation in amorphous carbon modifications, we have applied a nonorthogonal DF-based TB scheme for MD simulations¹⁰ of 128 carbon atom arrangements using fixed-volume cubic supercell arrangements of varying size in relation to the microscopic mass densities to be studied. The relaxation of the structures has been realized by applying two different cooling regimes of “dynamical quenching” character. We have performed a rapid quenching at a cooling rate of 10^{15} K/s over 2 ps as well as an extended stochastic cooling regime over 8 ps. In both cases, the relaxation started from a partly equilibrated liquid state of the model structures and followed a path of exponentially decreasing temperature. We solved Newton’s equations of motion using the Verlet algorithm. As characteristics of the first regime, we have rescaled the atomic velocities after each time step τ to an “instantaneous” temperature T required by the relaxation path, so that $\langle \frac{\vec{p}_i^2}{2M} \rangle = \frac{3}{2}k_B T$ holds for the mean kinetic energy per atom. Within the second regime, the rescaling of velocities is performed stochastically in time. A random generator produces equally distributed integer numbers n belonging to an interval $[1, n_{\max}]$. During a time period $n\tau$, the atoms can accelerate freely under influence of the interatomic forces. The rescaling procedure described above then is reapplied to the system. We have found that the stochastic quenching regime in any case produces more stable structures that are lower in energy than comparable systems obtained by the simple quenching dynamics.

As a reliable method for the calculation of interatomic forces, we used a DF scheme for the construction of a nonorthogonal TB potentials within the linear combination of atomic-orbitals formalism using the local-density approximation.¹¹ For details, we refer to Ref. 10. We express the Kohn-Sham orbitals ψ_i of the many-atom structures in terms of a minimal basis set of atom-centered localized valence electron orbitals: $\psi_i(\mathbf{r}) = \sum_{\nu} C_{\nu i} \phi_{\nu}^{\text{at}}(\mathbf{r} - \mathbf{R}_k)$. The basis functions are *eigenfunctions* of modified self-consistent single-atom calculations leading to pseudoatomic wave functions and potentials that are shrunk compared with a neutral atom. Making use of a simplified non-self-consistent two-center DF approach for solving the electron problem of the many-atom configuration, the total energy of the system as commonly accepted can be written as a sum over a band structure energy and a short-range repulsive two-particle potential, as described in Ref. 10. Although the method is as simple as well-established nonorthogonal parametrized TB schemes, it has been proven to be highly transferable to all-scale carbon and hydrocarbon structures.¹⁰ Interatomic forces can easily be derived from an exact calculation of the gradients of the total energy at the considered atom sites,

$$\begin{aligned} \mathbf{F}_l &= -\frac{\partial E_{\text{tot}}(\{\mathbf{R}_l\})}{\partial \mathbf{R}_l} \\ &= \sum_i n_i \sum_{\mu} \sum_{\nu} C_{\mu i} C_{\nu i} \left[-\frac{\partial H_{\mu\nu}}{\partial \mathbf{R}_l} + \varepsilon_i \frac{\partial S_{\mu\nu}}{\partial \mathbf{R}_l} \right] \\ &\quad - \frac{\partial E_{\text{rep}}}{\partial \mathbf{R}_l}. \end{aligned}$$

III. STABILITY AND PROPERTIES OF α -C MODELS VERSUS DENSITY

As the result of the simulation, we have obtained final metastable amorphous carbon modifications at different mass density. In all structures there is a clear tendency for the different hybrids to separate from each other and to form small interconnected subclusters. Owing to the fixed composition and constant atom number in the supercells, the cohesive energies at different densities have been compared to determine 3.0 g/cm^3 as a magic density at which most stable minimal energy amorphous carbon modifications are formed independent on the cooling regime applied. For an illustration we have plotted in Fig. 1 the calculated cohesive energies of all α -C model structures versus density including data of the rapid and extended stochastically cooled structures. For a reference the diamond cohesive energy per atom within the used DF-TB scheme is -8.02 eV . This confirms the stability of deposited high-density ta -C by different techniques.^{12–14}

In the following discussion we will focus mainly on

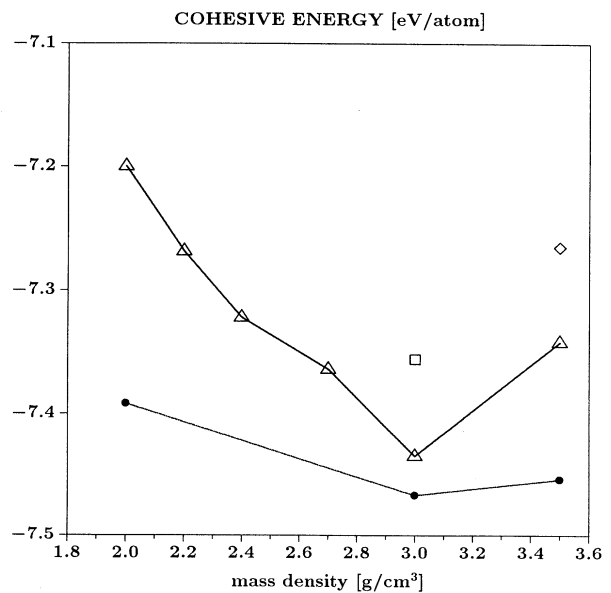


FIG. 1. Cohesive energies of amorphous carbon models vs density; rapid cooling (solid upper line), extended stochastic cooling (dotted lower line), 64-atom supercell *ab initio* MD (Ref. 5) (□), and 128-atom supercell generated similar to the WWW method (◇) (Ref. 19).

three densities, 2.0, 3.0, and 3.52 g/cm³ that are most interesting from the point of deposition and application; we will outline tendencies for changes in the vibrational behavior for densities in between. In a previous paper, we have already described how the structures and the related chemical bonding properties change with the simulation regime, and accordingly have been influenced in their energetic stability and global band gap properties.¹⁵

IV. VIBRATIONAL PROPERTIES: THEORETICAL BACKGROUND

For the vibrational analysis we have used fully relaxed amorphous model structures at different density obtained by conjugate gradient relaxation. The vibrational properties have been calculated within the harmonic approximation by construction of the dynamical matrix. By displacing each atom i by δr from its equilibrium position into the directions of the three basis vectors \vec{e}_α of the Cartesian coordinate system and into the corresponding opposite directions, one can calculate the elements $H_{ij}^{\alpha\beta}$ of the dynamical matrix using the forces $F_{j,\|\vec{e}_\beta}$ acting on each atom j into the directions \vec{e}_β :

$$H_{ij}^{\alpha\beta} = \frac{F_{j,\|\vec{e}_\beta}^- - F_{j,\|\vec{e}_\beta}^+}{2\delta r}.$$

The signs refer to the two possible displacements of atom i in the direction $\pm\vec{e}_\alpha$. As can be seen from a Taylor expansion of the total energy, the last equation eliminates errors of $O(\delta r)$ in the elements of H . To find a value for δr in practical applications, one has to consider two sources of errors: higher-order terms in the total energy expansion favoring a very small δr and the numeric instability of the above expression for very small displacements. We found $\delta r = 0.02a_B$ to be a reasonable choice.

After symmetrizing the dynamical matrix and projecting out translational and rotational modes, we solved the general eigenvalue problem

$$\mathbf{H}\vec{Y} = \omega^2\mathbf{M}\vec{Y},$$

where \mathbf{M} denotes a matrix with the atomic masses on the main diagonal while ω and \vec{Y} are the eigenvalues and their corresponding eigenvectors.

To illustrate the changing contributions of the different hybridized atoms to the total VDOS, we have used a projection technique. This allows us to show phonon densities of states splitted in hybrids to study the dynamical properties of the amorphous carbon networks at increasing mass density more in detail.

If \mathcal{H} denotes the set $\mathcal{H} = \{\nu_i\}_{i=1}^{M \leq 3N}$ of all indices of coordinates belonging to atoms of the same hybridization type, we can calculate the resulting hybrid phonon density of states,

$$g_{\mathcal{H}}(\omega) = \frac{1}{3N} \sum_{s \in \mathcal{H}} \sum_{i=1}^{3N} \delta(\omega - \omega_i) |\langle \vec{p}_s | \vec{Y}_i \rangle|^2,$$

where we have to sum over all elements of the index

set and $\langle \vec{p}_s | \vec{Y}_i \rangle$ is the scalar product of a vector $\vec{p}_s = (0, \dots, 0, 1, 0, \dots, 0)$ with the i th eigenvector \vec{Y}_i .

To discuss the localization behavior of the phonon modes, we have calculated an inverse participation ratio P_j^{-1} of the j th mode,

$$P_j^{-1} = \sum_{i=1}^{3N} |\langle \vec{p}_i | \vec{Y}_j \rangle|^4.$$

The usage of normalized eigenvectors guarantees the validity of the last expression and yielding the additivity of the various hybrid VDOS to the resulting total VDOS.

V. VIBRATIONAL SPECTRA: RESULTS

In Fig. 2, we present the calculated vibrational spectra of nine amorphous models generated by two different annealing regimes at various densities between 2.0 g/cm³ and 3.52 g/cm³. For reasons of comparison, all spectra have been convoluted by a constant resolution function. By using the projection technique, described in Sec. IV, we have decomposed the total vibrational

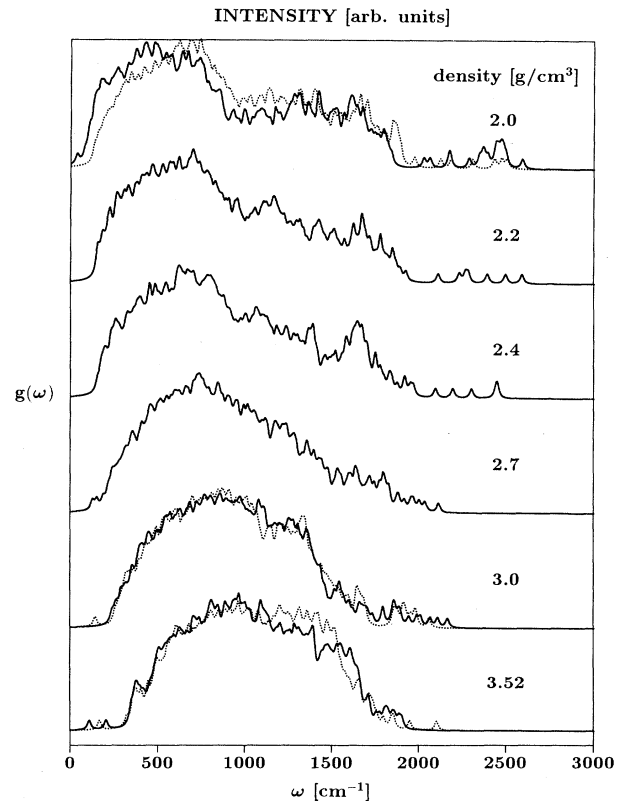


FIG. 2. Total vibrational density of states (VDOS) of amorphous carbon modifications vs mass density using identical broadenings as in Fig. 7; rapid cooling (solid line) and extended stochastic cooling (dotted line).

density of states into the different carbon hybrid contributions, which are shown in Figs. 3–5. This enables us to better analyze the chemical nature of the vibrational modes. Additionally, we have projected out structural defects by using the localization measure of the modes, which as inverse participation ratios have been defined in the preceding section, and now are plotted in Fig. 6 for all model structures.

For a detailed characterization of the differences in the vibrational behavior of the amorphous models in relation to the crystalline modifications, we show in Fig. 7 the theoretically calculated vibrational spectra of graphite and diamond using the same resolution function as for the amorphous spectra. While the diamond spectrum is split into one dominating peak area at 1300 cm^{-1} and four less intense features at 1000 , 900 , 700 , and 500 cm^{-1} , the graphite spectrum may be decomposed into two almost equally shaped main features, both linearly increasing, one from almost 0 to 850 cm^{-1} and the other from 1000 cm^{-1} to about 1700 cm^{-1} . The high-frequency bound in graphite is shifted relative to diamond due to an increased sp^2 stretching force.

Comparing now the amorphous modifications, the low-density a -C's (2.0 , 2.2 , 2.4) g/cm^3 are reminiscent of the graphitic-type behavior in the total broad frequency range up to 1800 cm^{-1} . Additionally, there is a considerable softening of the main low-frequency feature in

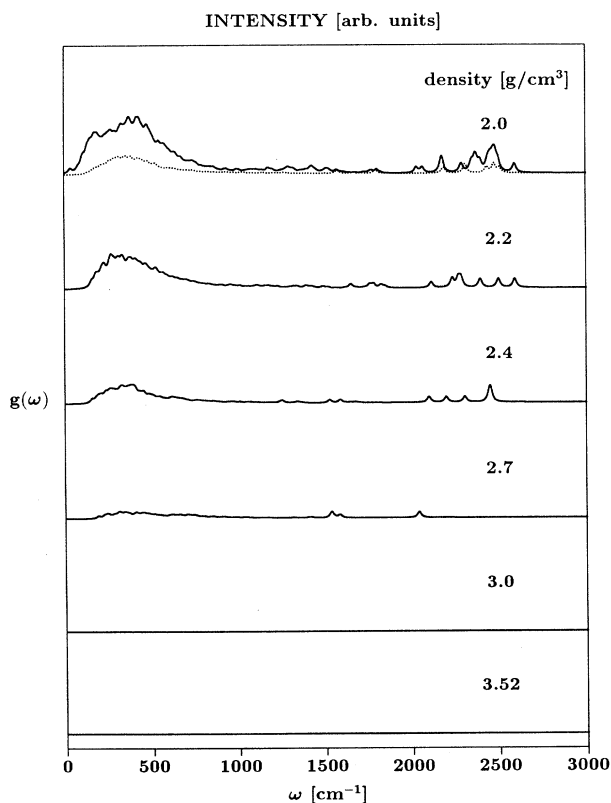


FIG. 3. sp -fractional VDOS of amorphous carbon vs mass density; same notations as in Fig. 2.

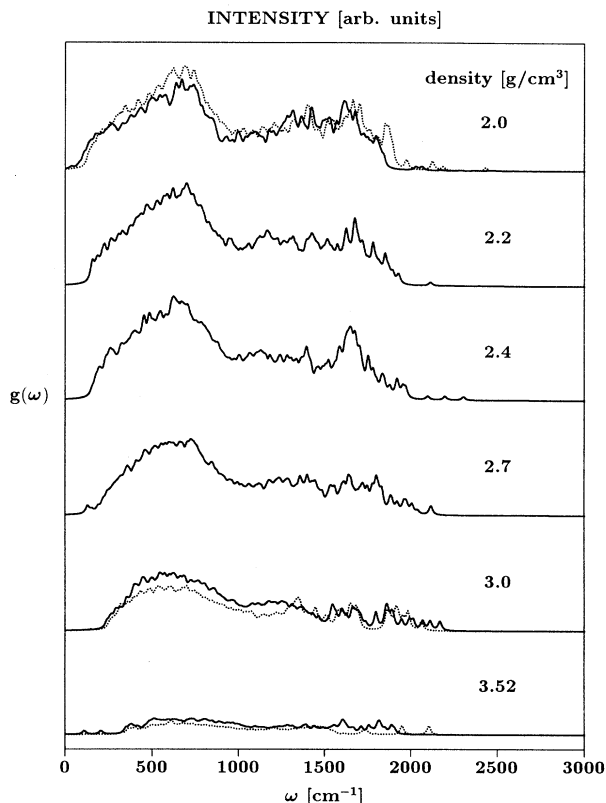


FIG. 4. sp^2 -fractional VDOS of amorphous carbon vs mass density; same notations as in Fig. 2.

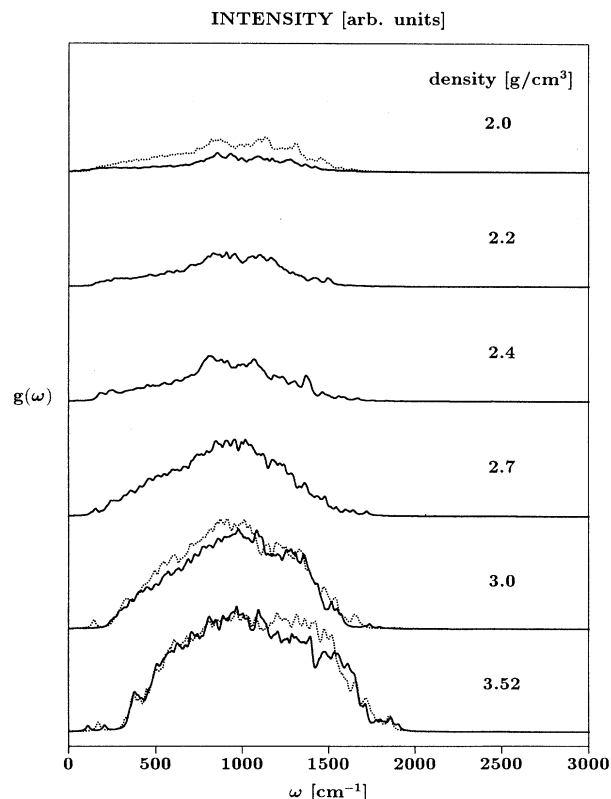


FIG. 5. sp^3 -fractional VDOS of amorphous carbon vs mass density; same notations as in Fig. 2.

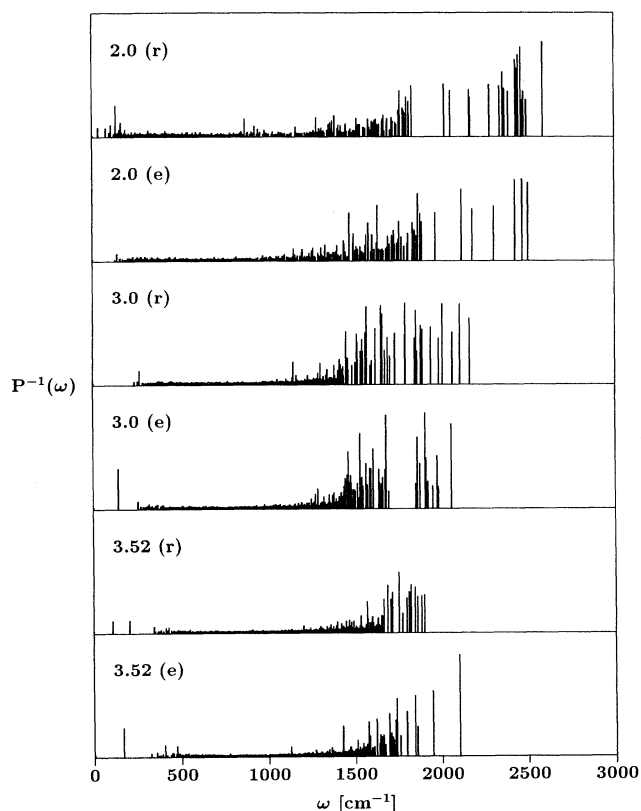


FIG. 6. Inverse participation ratio as localization measure of phonon modes of amorphous carbon vs mass density; rapid cooling (r) and extended stochastic cooling (e).

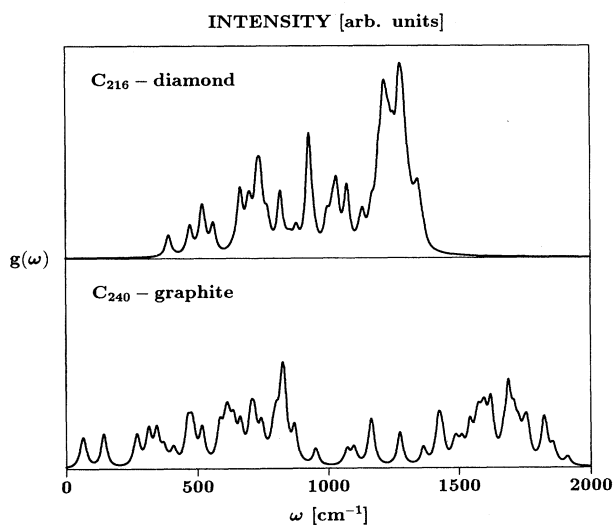


FIG. 7. Total vibrational density of states (VDOS) of diamond and graphite using a constant broadening of Lorentzian's $\delta = 40 \text{ cm}^{-1}$.

the rapid cooled 2.0 g/cm^3 sample. This softening appears due to chainlike sp - sp^2 segments and rings present in a low-connectivity network. As examples, we show in Fig. 8(a), a chain translational mode perpendicular to the chain axis at 105 cm^{-1} , and in 8(b) a corresponding ring translational mode at 147 cm^{-1} . There is a well-pronounced intensity drop at 1000 cm^{-1} in graphite separating high-frequency stretching vibrations from the lower-frequency spatial translational and bond-angle-changing modes. This is still obvious in the low-density structures up to 2.4 g/cm^3 and more and more is smoothed out with increasing density. The total frequency spread of the spectra is compressed to a range from 400 to 1600 cm^{-1} , where the spectra develop a characteristic half-sphere-shape, which is in support of recent VDOS calculations by Drabold *et al.*,⁵ and Wang and Ho.¹⁶ The softening of modes at higher densities is completely removed and the spectra lose all reminiscence of the splitted spectral graphite and diamond behavior.

Considering the fractional sp^2 and sp^3 VDOS, the intensities are correlated with the decreasing and increasing fractions of the related hybrids in the models, however, still preserving the overall shape and frequency range at all densities. The first broad feature in the sp^2 VDOS around 600 cm^{-1} as signature for extended alternating out-of-plane modes of clustered sp^2 units in rings and cross-linked chain segments, compare the two modes in Figs. 8(c) and 8(d) at 643 cm^{-1} and 600 cm^{-1} , respectively, is still visible up to diamond density. Opposite, the intensity of the higher-frequency sp^2 stretching vibrations is reduced considerably, now developing single localized modes above 1700 cm^{-1} . These modes refer to isolated sp^2 defects and paired sp^2 clusters within the rigid sp^3 matrix, see, e.g., a mode at 2100 cm^{-1} in Fig. 8(g).

At three densities, 2.0 , 3.0 , and 3.52 g/cm^3 , we compare the vibrational properties of models obtained at two different annealing cycles, as described in Sec. II. With increasing simulation time and the use of stochastic cooling at 2.0 g/cm^3 , the lowest frequency modes disappear. By decomposing the spectra into the different hybridized carbon contributions, this is mainly due to an almost complete removal of twofold coordinated sp atoms followed by a suppression of the sp -fraction VDOS in support of a higher network connectivity, an enhanced ring formation, and an increasing number of sp^3 sites. As a result, the intensity of the alternating out-of-plane modes of sp - sp^2 units around 600 cm^{-1} increases. Above 1600 cm^{-1} all modes become localized representing signs of structural defects, mostly arising as undercoordinated sp atoms in the higher-coordinated rigid amorphous matrix. Two examples of such localized modes, one sp - sp stretching at 2496 cm^{-1} and one sp - sp^2 stretching at 2430 cm^{-1} are shown in 8(e) and 8(f). With more extended relaxation time, the defect density is reduced in consistency with a reduced number of electronic defects discussed in Ref. 15 in relation to global band gap properties.

Analyzing the vibrational spectra of the 3.0 g/cm^3 models obtained at the two different annealing regimes, there is almost no change in both the total shape and the sp^x -fraction VDOS in consistency with a similar chemical

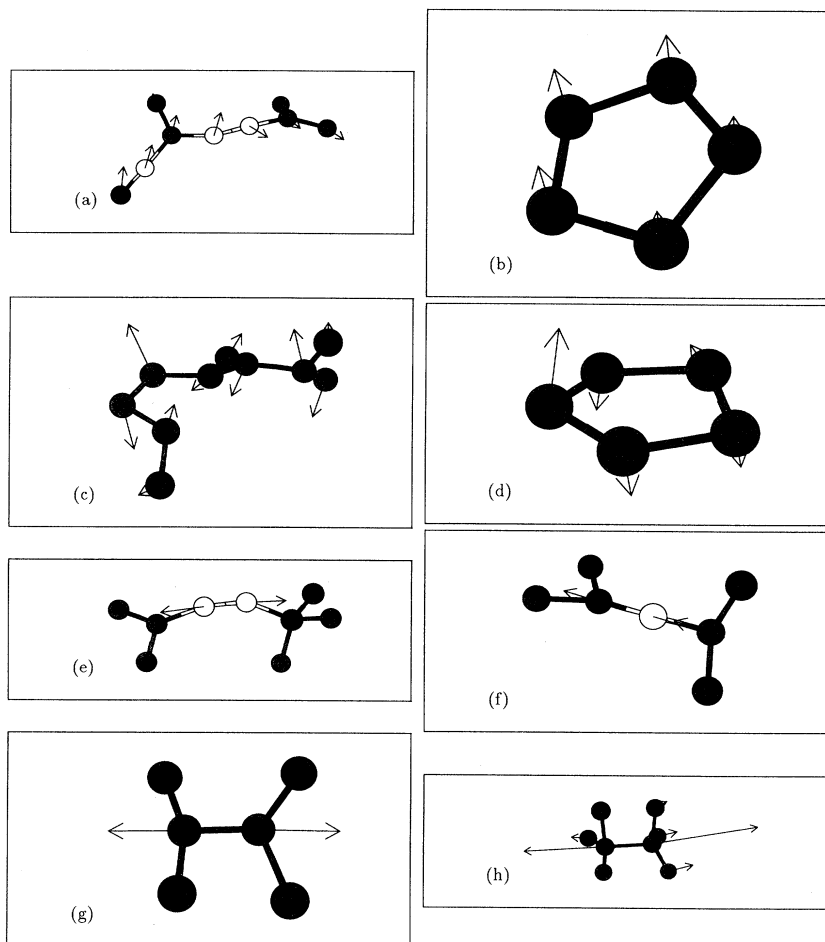


FIG. 8. Structural images of well-defined local and extended vibrational modes as described in the text.

composition.¹⁵ In both models, which are almost comparable in energy, see cohesive energy plot in Fig. 1, we find a favorably pairwise clustering of undercoordinated sp^2 atoms. At this density, the internal strain is maximally removed from the network favoring a minimal defect concentration. While the localized defect states in the models again are caused by the embedding of undercoordinated sp^2 units in a rigid sp^3 bonding environment, the overall width of the defect band is considerably reduced in the more extended cooled model. By using extended stochastic cooling regimes, the network stability is enhanced by increasing the cohesive energy and simultaneously minimizing the internal strain. As a result, strong inhomogeneities in the local strain are removed producing similar local environments for the embedding of isolated defects and π -bonded clusters.

Finally, the spectra of the two diamond-density amorphous models show a well-pronounced half-sphere-shape behavior. Again the sp^3 fraction slightly increases with extended relaxation time, which is reflected by the sp^x -fraction VDOS in Figs. 4 and 5. Simultaneously, the number of defects is reduced by the formation of three π -bonded sp^2 pairs producing three localized modes of sp^2 - sp^2 stretching type at 1700, 1950, and 2100 cm^{-1}

[compare Fig. 8(g)]. The frequency spread of these modes is due to varying local stress on the π bonds, indicating a nonuniform distribution even in such small supercells at diamond density. In the two high-density extended stochastically cooled structures, we find two additional localized low-frequency modes at (140–150) cm^{-1} . Both have identical origin and can be assigned to sp^3 -breathing modes of clustered sp^3 units, schematically depicted in Fig. 8(h), which are confined within a rather stiff and rigid bonding environment. Comparing once more the spectra of the diamond-density amorphous carbon with that of diamond, the steep intensity drop at 1100 cm^{-1} is completely smoothed out, developing the already-mentioned characteristic half-sphere-shaped spectra in the high-density amorphous modifications. Additionally, there is a shift of the high-frequency edge from 1300 to 1600 cm^{-1} .

The loss in the reminiscence of the splitted spectral diamond-lattice behavior, which is different from amorphous silicon,¹⁷ further may be analyzed by considering the fractional sp^x VDOS. While the sp^2 VDOS preserves the extended out-of-plane features between 500 and 900 cm^{-1} and splits into isolated localized modes at higher frequency, the sp^3 VDOS at all densities by itself devel-

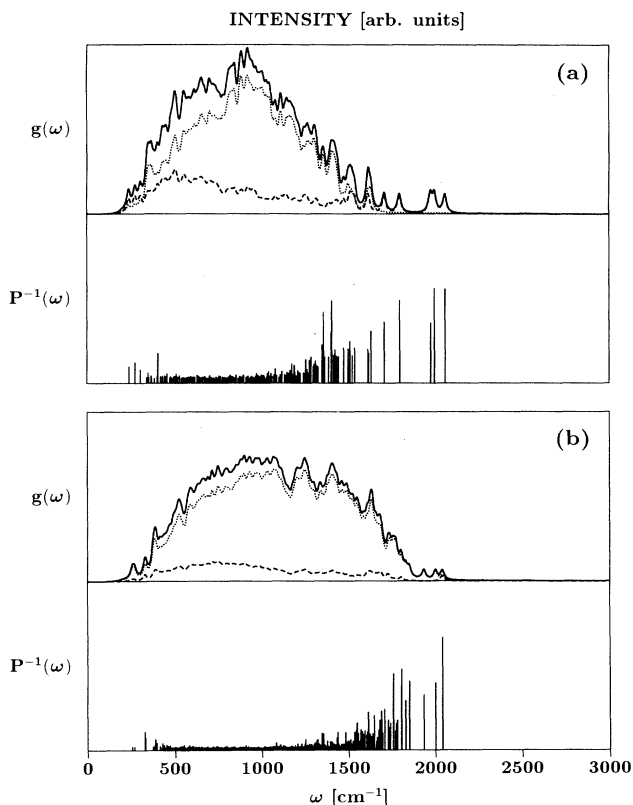


FIG. 9. Total, sp^2 -fractional VDOS and inverse participation ratio (a) of a 64-atom amorphous carbon supercell at 3.0 g/cm^3 , obtained by the Sankey/Drabold code and (b) of a 128-atom amorphous carbon supercell at diamond-density generated similar to the Monte Carlo WWW method.

opes a half-sphere-shape. The strong crystalline diamond stretching feature at 1300 cm^{-1} and the intensity drop at 1100 cm^{-1} is completely smoothed out in the amorphous spectra. This qualitatively may be explained due to the relative large local bond length and bond-angle distortions of the strained sp^3 matrix at high density, $\Delta R = \pm 0.6\text{--}0.8 \text{ \AA}$ and $\Delta\Theta = \pm 10.4\text{--}12.3^\circ$, respectively,¹⁵ but still needs further quantitative study.

To support our findings, we have compared the spectra of our high-density models with that of a 64-atom cell obtained at 3.0 g/cm^3 by the Sankey/Drabold code⁵ in Fig. 9(a) and that of a 128-atom cell generated similar to the Monte Carlo (WWW) method^{18,19} in Fig. 9(b). As can be seen, the two spectra show almost identical behavior in shape and localization as the related spectra of the 128-atom supercell obtained by the DF-MD method. Before calculating the VDOS, both structures have been finally relaxed to $T = 0 \text{ K}$ using conjugate gradient methods within our DF-TB scheme.¹⁰

VI. SUMMARY, COMPARISON WITH EXPERIMENTAL DATA

We have presented vibrational signatures of amorphous carbon at various densities, which may be used for com-

parison with experimental data. While there is limited Raman data of $a\text{-C}$ samples,⁶ almost all IR studies have been performed on hydrogenated amorphous carbon, $a\text{-C:H}$.⁷ However a clear assignment of the modes obtained from the atomic-scale models to the most characteristic experimental features can be given. As discussed by Tamor and Vassel,⁶ the Raman spectra of amorphous carbon films exhibit two graphite-related broad features at approximately 1550 cm^{-1} (G line) and 1350 cm^{-1} (D line) and an additional third one centered at 600 cm^{-1} . All three features have correspondingly related images in the sp^2 -fractional VDOS of the models in the same frequency range for all densities up to 3.0 g/cm^3 (compare Fig. 4). The additional occurring third feature, which never could be observed in hydrogenated structures, recently has been discussed by Wang and Ho¹⁶ to represent characteristic out-of-plane sp^2 modes. From a localization analysis, we support the findings of Wang and Ho. While the spatial out-of-plane low-frequency sp^2 modes, shown in panel 8(c) and 8(d), around 600 cm^{-1} remain extended, the high-frequency stretching vibrations [Figs. 8(e)–8(g)] above 1500 cm^{-1} become strongly localized, which is due to their embedding in a higher-coordinated rigid-bonding environment. The highest frequency localized modes at low densities extending to $2400\text{--}2500 \text{ cm}^{-1}$ indicate isolated sp clusters sparsely distributed in a higher-coordinated rigid bonding environment. By the picking of modes at well-defined frequencies, shown in Fig. 8, we confirm Tamor and Vassel's discussion and relate the broad high-frequency feature, occurring in low-density $a\text{-C}$ around 1500 cm^{-1} , to complex extended stretching modes of the sp^2 matrix. As recently discussed by Drabold *et al.*,⁵ and Wang and Ho,¹⁶ these stretching modes become localized at higher density by changing from a sp^2 to a sp^3 matrix, separating now smaller sp^2 clusters. While this delocalization to localization transition can be established for the higher-frequency range, all modes belonging to the low-frequency feature around 600 cm^{-1} remain delocalized even at highest densities representing in all cases out-of-plane modes of all-scale cross-linked sp^2 chainlike segments and rings.

Additionally, the upward shift of the spectral features in the extended stochastically cooled modification at 2.0 g/cm^3 consistent with a related shift of the graphite G line in samples deposited at higher substrate temperature as discussed by Tamor and Vassel,⁶ is a reflection of the enhanced stiffening of the host matrix combined with a reduction of the phonon mode softening. Recent progress in Raman investigations of amorphous carbon at various density²⁰ will further stimulate our efforts in calculating Raman intensities for the amorphous models.

ACKNOWLEDGMENTS

We gratefully acknowledge support from the Deutsche Forschungsgemeinschaft (DFG) and Deutscher Akademischer Austauschdienst (DAAD). Sincere thanks are due to D. A. Drabold and R. Cappelletti for stimulating discussions and the Physics and Astronomy Department at Ohio University, Athens, for support and hospitality during a stay at OU.

- ¹ J. Robertson, *Diamond Relat. Mater.* **2**, 984 (1993).
- ² G. Galli, R. M. Martin, R. Car, and M. Parrinello, *Phys. Rev. B* **42**, 7470 (1990).
- ³ C. Z. Wang, K. M. Ho, and C. T. Chan, *Phys. Rev. Lett.* **70**, 611 (1993).
- ⁴ Th. Frauenheim, P. Blaudeck, U. Stephan, and G. Jungnickel, *Phys. Rev. B* **48**, 4823 (1993).
- ⁵ D. A. Drabold, P. A. Fedders, and P. Stumm, *Phys. Rev. B* **49**, 16 415 (1994).
- ⁶ M. A. Tamor and W. C. Vassell, *J. Appl. Phys.* (to be published).
- ⁷ S. R. P. Silva, G. A. J. Amaratunga, and C. P. Constantino, *J. Appl. Phys.* **72**, 1149 (1992).
- ⁸ U. Stephan, Th. Frauenheim, P. Blaudeck, and G. Jungnickel, *Phys. Rev. B* **49**, 1489 (1994).
- ⁹ Th. Frauenheim, G. Jungnickel, U. Stephan, P. Blaudeck, S. Deutschmann, M. Weiler, S. Sattel, K. Jung, and H. Ehrhardt, *Phys. Rev. B* **50**, 7940 (1994).
- ¹⁰ D. Porezag, Th. Frauenheim, Th. Köhler, G. Seifert, and R. Kaschner, *Phys. Rev. B* (to be published).
- ¹¹ G. Seifert and H. Eschrig, *Phys. Status Solidi B* **127**, 573 (1985); G. Seifert, H. Eschrig, and W. Bieger, *Z. Phys. Chem. (Leipzig)* **267**, 529 (1986); G. Seifert and R. O. Jones, *Z. Phys. D* **20**, 77 (1991).
- ¹² D. R. McKenzie, D. Muller, and P. A. Pailthorpe, *Phys. Rev. Lett.* **67**, 773 (1991).
- ¹³ G. Jungnickel, M. Kühn, S. Deutschmann, F. Richter, U. Stephan, P. Blaudeck, and Th. Frauenheim, *Diamond Relat. Mater.* **3**, 1056 (1994).
- ¹⁴ M. Weiler, S. Sattel, K. Jung, H. Ehrhardt, and V. S. Veerasamy, *Diamond Relat. Mater.* **3**, 608 (1994); M. Weiler, S. Sattel, K. Jung, H. Ehrhardt, and J. Robertson (unpublished).
- ¹⁵ Th. Frauenheim, G. Jungnickel, Th. Köhler, and U. Stephan, *J. Non-Cryst. Solids* **182**, 186 (1995).
- ¹⁶ C. Z. Wang and K. M. Ho, *Phys. Rev. Lett.* **71**, 1184 (1993).
- ¹⁷ I. Stich, R. Car, and M. Parrinello, *Phys. Rev. B* **44**, 11 092 (1991).
- ¹⁸ F. Wooten, K. Winer, and D. Weaire, *Phys. Rev. Lett.* **54**, 1392 (1985).
- ¹⁹ G. Jungnickel, Doctoral thesis, Technische Universität Chemnitz, 1994; G. Jungnickel, Th. Köhler, U. Stephan, and Th. Frauenheim, *Diamond Relat. Mater.* (to be published).
- ²⁰ V. Mirkulov and J. S. Lannin, in *Physics of Semiconductors: Proceedings of the XXII International Conference*, edited by D. J. Lockwood (World Scientific, Singapore, 1995), p. 2681.